The following publication Pengcheng Zhao, Hoi Lut Ho, Wei Jin, Shangchun Fan, Shoufei Gao, Yingying Wang, and Pu Wang, "Gas sensing with mode-phase-difference photothermal spectroscopy assisted by a long period grating in a dual-mode negative-curvature hollow-core optical fiber," Opt. Lett. 45, 5660-5663 (2020) is available at https://doi.org/10.1364/OL.404323.

Gas sensing with mode-phase-difference photothermal spectroscopy assisted by a long period grating in a dual-mode negative-curvature hollow-core optical fiber

PENGCHENG ZHAO[1,2,3], HOI LUT HO[2,3], WEI JIN[2,3,7], SHANGCHUN FAN[1,4,8], SHOUFEI GAO[2], YINGYING WANG[5], AND PU WANG[6]

[1] *School of Instrumentation and Optoelectronic Engineering, Beihang University, Beijing, China.*
[2] *Department of Electrical Engineering and Photonics Research Center, The Hong Kong Polytechnic University, Hong Kong, China.*
[3] *Photonics Research Center, The Hong Kong Polytechnic University Shenzhen Research Institute, Shenzhen, China.*
[4] *Beijing Advanced Innovation Center for Big Data-Based Precision Medicine, Beihang University, Beijing, China.*
[5] *Institue of Photonics Technology, Jinan University, Guangzhou, China*
[6] *Beijing Engineering Research Centre of Laser Technology, Beijing University of Technology, Beijing, China.*
[7] *eewjin@polyu.edu.hk*
[8] *shangcfan@buaa.edu.cn*

We demonstrate sensitive gas detection with mode-phase-difference photothermal spectroscopy assisted by a long period grating (LPG) inscribed on a dual-mode negative-curvature hollow-core fiber (NC-HCF). The LPG is inscribed using a pulsed CO_2 laser, which enables pump propagation in the fundamental LP_{01} mode to achieve maximum photothermal phase modulation while excites both the LP_{01} and LP_{11} modes at the probe wavelength to form an dual-mode interferometer for the detection of the phase difference. With a 1533 nm pump and a 1620 nm probe, a noise-equivalent-concentration of ~2.2 ppb acetylene is achieved with an 85-cm-long NC-HCF gas cell and 1 s lock-in time constant.

Photothermal interferometry (PTI) is an ultra-sensitive method for trace gas detection [1]. A pump-and-probe configuration is typically used [2, 3]: pump absorption induces localized heating, modulates the refractive index (RI) of gas medium and hence the accumulated phase of the probe beam, which is detected by optical interferometry. Early PTI systems were implemented with free-space optics [2–6]. The development of micro-structured hollow-core fibers (HCFs) allows tight confinement of pump and probe beams as well as gas sample simultaneously in the hollow-core, enabling strong light-gas interaction over a long distance. With HCF gas cells, gas detection with noise equivalent concentration (NEC) down to parts per billion (ppb) level has been demonstrated using near infrared lasers as pump and probe sources and different phase detection schemes, including Mach-Zehnder [7], Sagnac [8] and Fabry-Perot interferometers [9, 10].

Recently, we demonstrated a mode-phase-difference photothermal spectroscopy (MPD-PTS) technique by use of a dual-mode negative-curvature HCF (NC-HCF) and achieved parts per trillion (ppt) level NEC [11]. The technique detects the modulation of the differential phase between the LP_{01} and LP_{11} modes, which is sensitive to gas absorption in the hollow-core but insensitive against external perturbations. The differential photothermal phase modulation is proportional to gas concentration C and can be expressed as [11]

$$\delta\phi = \Delta\phi_{01} - \Delta\phi_{11} \approx k^*(\eta, f)\alpha\left(\lambda_{\text{pump}}\right) CLP_{\text{pump}} \quad \textbf{(1)}$$

where $\alpha\left(\lambda_{\text{pump}}\right)$ is the gas absorption coefficient, λ_{pump} the pump wavelength, L the length of the HCF, P_{pump} the average pump power in the HCF, η the fractional pump power in the LP_{01} mode, f the pump modulation frequency, and k^* the phase modulation coefficient that is related to η and f. Calculation shows that the differential phase modulation is maximized with η = 100%, meaning that it is preferable to launch all the pump power into the LP_{01} mode. However, to detect the differential phase modulation, two probe modes, i.e., both LP_{01} and LP_{11} modes, need to be excited in the NC-HCF to form a dual-mode interferometer. Previously, we constructed the probe interferometer by offset alignment to respectively excite and combine the two probe modes at the input and output ends of the NC-HCF [11]. However, the offset alignment excites two modes indiscriminately for the pump and the probe, resulting in reduced pump power in the LP_{01} mode and hence the photothermal differential phase modulation. In addition, to optimize the efficiency of detecting the differential phase modulation, it is preferred to equalize the optical power levels in the two probe modes to achieve maximum fringe contrast. This requires precise control of the offsets between the HCF and the input/output single mode fibers (SMFs), which makes the optical alignment complex and time consuming.

In this letter, we demonstrate the inscription of a long period grating (LPG) in a dual-mode NC-HCF, which selectively couples the LP_{01} to LP_{11} mode at probe wavelength but not the pump wavelength. With such a LPG, we construct a dual-mode HCF interferometer to probe the differential phase modulation without the need for an offset at the input SMF/HCF splice joint. This simplifies the optical alignment procedure and at the same time allows the propagation of the pump power only in the LP_{01} mode of the HCF, maximizing the differential photothermal phase modulation and enabling high sensitivity gas detection with a lesser complex system.

The scanning electron micrograph (SEM) cross-section of the NC-HCF used in our experiment is shown in Fig. 1(a). It includes a ring-shaped silica cladding with outer diameter of ~203 µm and inner diameter of ~60 µm, 7 capillary rings with diameter of ~15 µm and thickness of ~370 nm. The inscribed air-core has a diameter of ~30 µm. Mode analysis was conducted with COMSOL Multiphysics using a SEM-based geometry model as illustrated in Fig. 1(b). The fiber supports two groups of modes: the LP_{01}-like mode (Fig. 1(c)) and a pair of LP_{11} modes that are labelled as LP_{11a} and LP_{11b} modes (Figs. 1d and 1e respectively). The dispersion relationships are shown in Fig. 1(f), and the effective RI difference between LP_{01} and LP_{11} modes is $\sim 1.1 \times 10^{-3}$ at 1620 nm. The modal beat lengths as functions of wavelength are shown in Fig. 1(g).

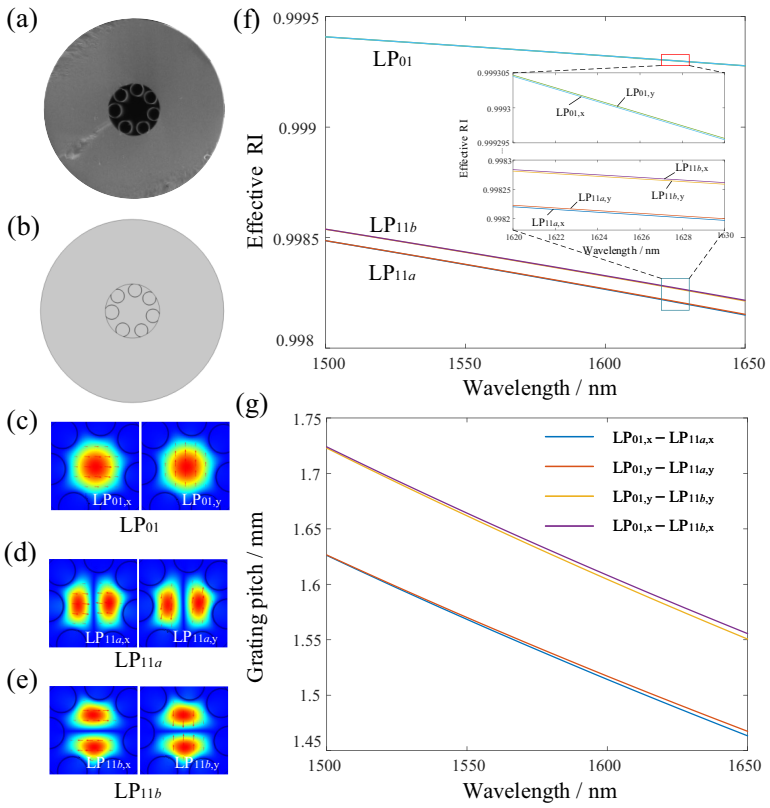

Fig. 1. (a) SEM cross-sectional image of the NC-HCF. (b) SEM-based geometry model of the NC-HCF for mode analysis. (c-e) Electric field distributions of LP_{01}, LP_{11a} and LP_{11b} modes with two orthogonal polarizations. (f) Calculated effective RI versus wavelength for two groups of modes in NC-HCF. Inset: zoom-up images in the wavelength range of 1620 to 1630 nm (g) Calculated grating pitches (modal beat lengths) against the wavelength for coupling from LP_{01} to LP_{11a} and LP_{11b} modes.

Theoretically if a LPG is made along the NC-HCF with grating pitch Λ equaling the modal beat length, i.e. the phase matching occurs, the energy will couple resonantly from one mode to another. For the LP_{01} and LP_{11} modes discussed above, the wavelength λ_{res} at which the resonant coupling occurs may be expressed as [12]:

$$\lambda_{res} = (n_{01} - n_{11})\,\Lambda \tag{2}$$

where n_i (i=01 or 11) is the effective RI of the respective LP mode. The grating pitch required for mode conversion at a specific wavelength may be obtained from Fig. 1(g), which will be used as a guide for LPG fabrication. For example, if we wish to convert LP_{01} to LP_{11a} or LP_{11b} at ~1628 nm, the grating pitch would be ~1.486 or ~1.578 mm.

A LPG on an optical fiber may be fabricated by heat treatment of the fiber with CO_2 laser irradiation [13], arc discharge [14], hydrogen-oxygen flame [15] or by mechanical micro-bending[16]. These techniques have been applied successfully to inscribe LPGs in conventional optical fibers[13, 15–17], solid-core photonic crystal fibers [16, 18, 19] as well as hollow-core photonic bandgap [20, 21]and anti-resonant fibers [22]. However, inscription of a LPG along an NC-HCF was not reported to our knowledge.

Here we use a pulsed CO_2 laser to inscribe a LPG on an NC-HCF and the experimental setup is shown in Fig. 2(a). The NC-HCF is fusion spliced to a SMF at the input end. Since the NC-HCF can support two groups of modes, it is important to align the cores of the SMF and NC-HCF as accurately as possible to excite ideally only the LP_{01} mode. Light from a broadband source (Amonics,

ALS-CWDM-FA) is launched into the NC-HCF from the input SMF and the output spectrum from the NC-HCF is monitored with optical spectrum analyzer (OSA, Yokogawa-AQ6317B). The CO_2 laser is scanned across the NC-HCF transversely and periodically along the HCF to periodically deform the HCF to form a LPG [23, 24]. The CO_2 laser system (SYNRAD 48-1) works in a pulsed mode with the following settings: average output power ~9W, repeat frequency 10 kHz, the line speed of the scanning 1 mm/s, and Q-release time 90 μs, diameter of laser spot ~50 μm. During the LPG fabrication, an 80 g mass was applied to keep NC-HCF straight and improve the writing efficiency.

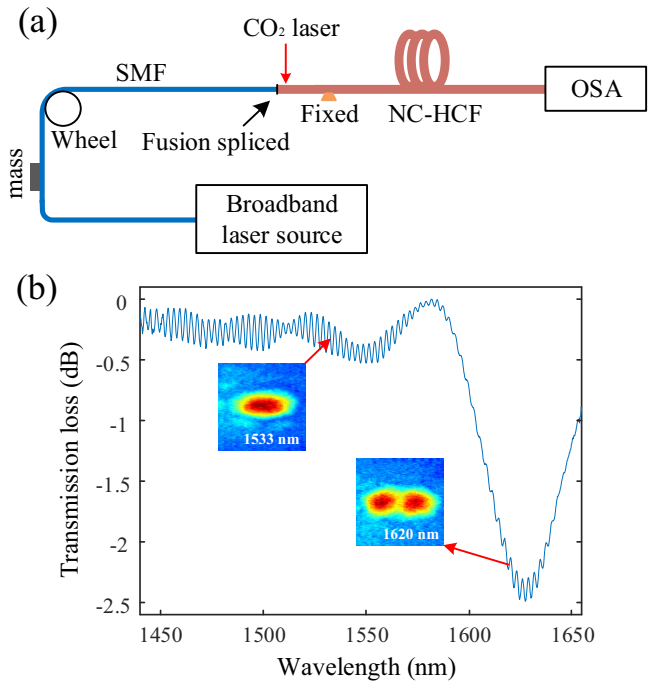

Fig. 2. (a) Experimental set-up for LPG fabrication. (b) The transmission spectrum of a LPG with 29 grating periods and grating pitch of ~1.44 mm. Insert: Intensity distributions viewed at output end of NC-HCF.

Fig. 2(b) shows the transmission spectrum of a LPG inscribed on an 85-cm-long NC-HCF. The LPG has 29 grating periods and a grating pitch of ~1.44 mm, giving a grating length of ~4.2 cm. The LPG is at the end of the NC-HCF near the SMF/HCF joint. The transmission spectrum is recorded by OSA with wavelength resolution of ~1 nm, and average insert loss around 1533 nm is ~0.33 dB. The LPG has a resonance dip at ~1628 nm with the depth of ~2.2 dB, which is caused by relatively large transmission loss of the LP_{11} mode. This resonance dip is believed due to coupling to the LP_{11a} mode and it is noted that the grating pitch used in the experiment is slightly smaller than the calculated value of ~1.486 mm. The discrepancy may be due to the geometry model is not exactly the same as the actual NC-HCF and the CO_2 laser irradiation may modify the mode fields as well as the effective RIs of the modes [24]. According to Fig. 1(g), the resonant wavelength for coupling to LP_{11b} mode is much longer and well beyond 1650 nm. The dense fringes are due to the interference of the LP_{01} and LP_{11} modes at the output of the NC-PCF, because the coupled LP_{11} mode is not completely attenuated at the output. The near-field mode intensity images are examined at the output of the NC-HCF using infrared CCD camera, and typical results at and away from the grating resonant wavelength are shown in the inserts. We can see that, with the help of LPG, the optical power is primarily in the LP_{01} mode at ~1533 nm while considerable optical power is in the LP_{11} mode at ~1620 nm. Therefore, if we use a pump around 1533 nm and a probe at 1620 nm, we should be able to keep the pump power mainly in the LP_{01} mode, while distribute the probe power approximately equally in the LP_{01} and LP_{11} mode to form a high-contract in-fiber modal interferometer.

A gas cell was constructed with the above said NC-HCF with a LPG on it, which is shown in Fig. 3(a). As mentioned earlier, the input SMF is well-aligned and fusion spliced to the HCF so that both pump and probe beams from the SMF are launched ideally into the LP_{01} mode of the HCF. After passing through the LPG, the pump light remains in the LP_{01} mode; however, the probe light is partially converted into LP_{11} mode and hence both LP_{01} and LP_{11} modes of the probe are propagating in the HCF. At the output end, the HCF is mechanically jointed with a SMF with ceramic ferrules and a sleeve. A lateral core-offset of a few μm is introduced at the output HCF/SMF joint so that the output SMF collects light from both LP_{01} and LP_{11} of the probe to form an in-fiber dual-mode interferometer to detect the differential photothermal phase modulation. Such a configuration offers at least two advantages: (i) it ensures that the pump power is always in the LP_{01} mode so that the photothermal phase modulation is maximized [11] and (ii) the input alignment procedure is considerably simplified while the fringe contrast can still be maximized by optimizing the offset at the output joint. A small air-gap is kept between the ends of the HCF and SMF for gas filling into the HCF. The mechanical joint is fixed with AB glue and sealed in a plastic tube with an inlet and an outlet for gas filling. The NC-HCF is looped with a diameter of ~20 cm.

Fig. 3(b) shows the transmission spectrum of the modal interferometer, which is measured with broadband source and an OSA with wavelength resolution of 50 pm. The average insertion loss of the SMF-LPG-HCF-SMF structure around 1620 nm is ~11 dB,

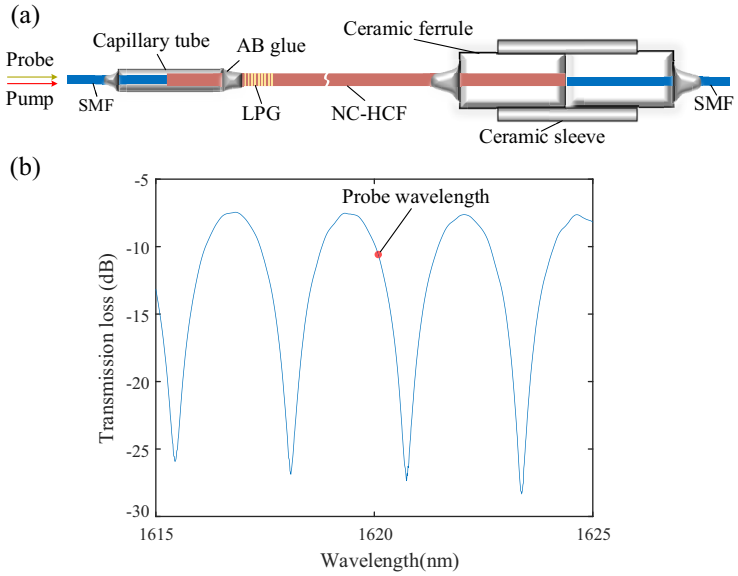

Fig. 3. (a) The SMF-LPG-HCF-SMF assembly as the gas cell as well as a dual-mode interferometer for detecting differential mode-phase modulation. (b) Measured transmission spectrum of the dual-mode interferometer.

which is primarily due to the offset mechanical joint. The free spectral range (FSR) and contrast of the interference fringes are ~2.5 nm and ~20 dB, respectively.

The entire experimental setup for gas detection is shown in Fig. 4. Pump light comes from a 1.53-μm distributed feedback (DFB) laser, and its wavelength is scanned slowly across the P(13) absorption line of acetylene at ~1532.83 nm and at the same time sinusoidally modulated at a higher frequency f of ~11 kHz to produce photothermal phase modulation. To maximize the second harmonic ($2f$) signal, the depth of wavelength modulation is chosen to be ~2.2 times the linewidth of the P(13) line [25]. Probe light is from an external cavity diode laser (ECDL), and its wavelength is tuned to a quadrature point of the dual-mode interference fringe around 1620 nm, as indicated in Fig. 3(b), for efficient detection of the differential phase modulation. The pump and probe beams are launched into the NC-HCF through a wavelength-division multiplexer (WDM1), and the probe beam coming out from WDM2 is detected by a photodetector (PD). The $2f$ component of the differential phase modulation of the probe is demodulated by a lock-in amplifier (LIA) and transmitted to a computer via a data acquisition (DAQ) card for further processing.

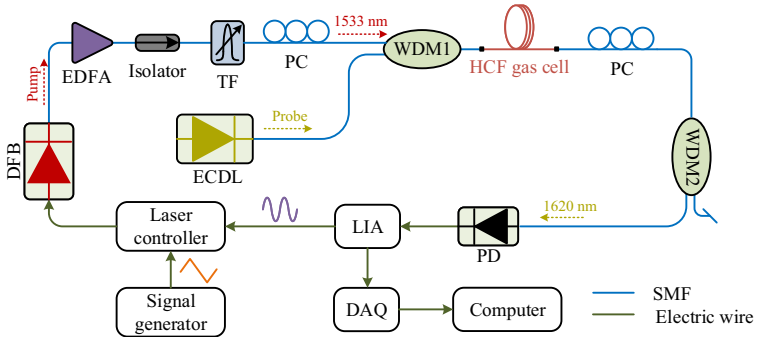

Fig. 4. Experimental set-up for gas detection with a ~85-cm-long NC-HCF. ECDL, external cavity diode laser (the probe); DFB, distributed feedback laser (the pump); EDFA, erbium-doped fiber amplifier; TF, tunable optical filter to minimize EDFA's amplified spontaneous emission noise; WDM1-WDM2, wavelength-division multiplexers; PC, polarization controller; LIA, lock-in amplifier; DAQ, data acquisition; PD, photo-detector.

Gas detection experiment was conducted by filling the NC-HCF gas cell with calibrated 500 ppb acetylene balanced by argon. Fig. 5(a) shows the $2f$ lock-in output signal when the pump is tuned across the P(13) line of acetylene with different pump powers. Fig. 5(b) shows the peak-to-peak $2f$ signal and 1σ noise as functions of pump power levels. We calculated the 1σ noise value based on recorded 3-minute noise data when the pump wavelength is fixed at ~1533.06 nm, away from P(13) absorption line. With ~235 mW pump power from input SMF, NEC is calculated to be ~2.2 ppb acetylene with 1s time constant at room temperature and pressure of ~1 bar, corresponding to a noise equivalent absorption (NEA) of $\sim 2.3 \times 10^{-9}\text{cm}^{-1}$. Alan-Werle deviation analysis [26, 27] was carried out with noise data over a period of 1.5 hours, and the results are shown in Fig. 5(c). The NEC goes down to ~600 ppt with averaging time of 100 s, corresponding to NEA of $\sim 6.3 \times 10^{-10}\text{cm}^{-1}$. Comparing with the results in Ref. [11] and considering the effects of different gas pressure, length of NC-HCF and input pump power level used in the two experiments, the normalized NEC per unit

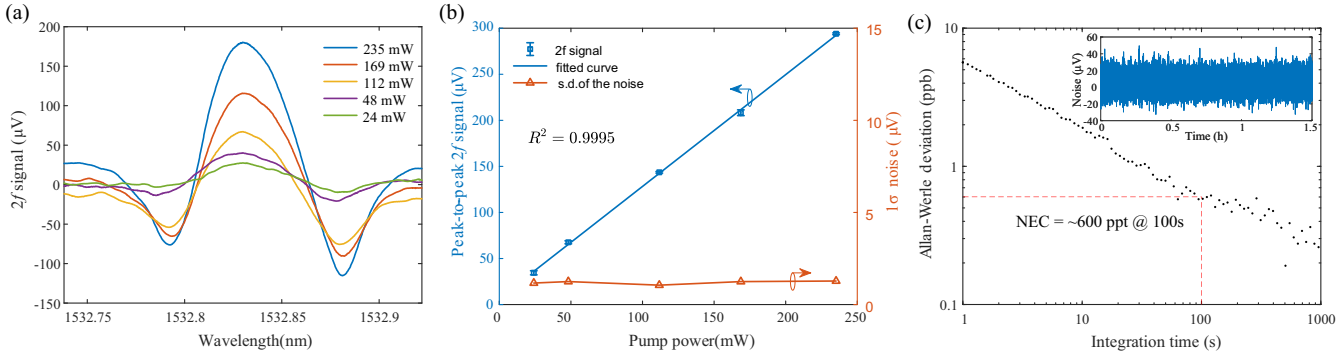

Fig. 5. Experimental results for a ~85-cm-long NC-HCF. (a) The PT signal ($2f$ signal) with pump wavelength tuned across the P(13) line of C_2H_2. (b) The peak-to-peak value of the $2f$ signal and the 1σ noise as functions of pump power levels. Error bars show the s. d. from five measurements. The mean probe power on the PD is -7 dBm. The lock-in time constant of 1 s and filter slope is 18 dB Oct^{-1}, corresponding to 0.094 Hz detection bandwidth. (c) Allan-Werle deviation plot based on noise data over a period of 1.5 hours, which is shown in the inset, and the lock-in time constant is 30 ms, corresponding to 0.28 Hz detection bandwidth. All data are obtained at room temperature and pressure of ~1 bar.

pump power, fiber length and gas pressure is ~1.4 time better for the present work.

In summary, we have reported the fabrication of LPG on an NC-HCF and constructed a LPG assisted NC-HCF gas cell to achieve sensitive gas detection performance with the mode-phase-difference photothermal spectroscopy. The use of a LPG instead of offset alignment to form the probe interferometer for differential mode-phase detection simplifies the construction of gas cell and maximizes the differential photothermal phase modulation, which enables high performance with a simpler system. Preliminary experiments with a 85-cm-long NC-HCF gas cell demonstrated a noise equivalent gas concentration of sub-ppb-level acetylene with an averaging time of 100 s, which could be further improved by using a longer length of NC-HCF and by increasing the pump power level in the hollow-core. A properly designed NC-HCF could transmit pump light from visible to MIR, which, when combined with the LPG based in-fiber probe modal interferometer in the NIR, would enable all-fiber cost-effective and ultra-sensitive gas sensors for a range of practical applications.

Funding. Hong Kong SAR government (GRF 15260316), National Natural Science Foundation of China (61827820, 61535004, 61675011), The National Key Research and Development Program of China (2019YFB2203904), The Hong Kong Polytechnic University (YW4C, SB95 and 4-BCD1),the Program for Changjiang Scholars and Innovative Research Team in University (grant-IRT_16R02), Research program of Beijing Municipal Education Commission (KZ201810005003).

Acknowledgments. This work was carried out at HK PolyU, and we also thank the support from State Key Laboratory of Advanced Optical Communication Systems and Networks, China.

Disclosures. The authors declare no conflicts of interest.

REFERENCES

1. S. E. Bialkowski, *Photothermal spectroscopy methods for chemical analysis*, vol. 177 (John Wiley & Sons, 1996).
2. C. C. Davis and S. J. Petuchowski, Appl. Opt. **20**, 2539 (1981).
3. M. A. Owens, C. C. Davis, and R. R. Dickerson, Anal. Chem. **71**, 1391 (1999).
4. K. H. Fung and H. B. Lin, Appl. Opt. **25**, 749 (1986).
5. J. P. Waclawek, C. Kristament, H. Moser, and B. Lendl, Opt. Express **27**, 12183 (2019).
6. K. Krzempek, A. Hudzikowski, A. Głuszek, G. Dudzik, K. Abramski, G. Wysocki, and M. Nikodem, Appl. Phys. B **124**, 74 (2018).
7. W. Jin, Y. Cao, F. Yang, and H. L. Ho, Nat. Commun. **6**, 1 (2015).
8. Y. Lin, W. Jin, F. Yang, Y. Tan, and H. L. Ho, Opt. Lett. **42**, 4712 (2017).
9. F. Yang, Y. Tan, W. Jin, Y. Lin, Y. Qi, and H. L. Ho, Opt. Lett. **41**, 3025 (2016).
10. H. Bao, Y. Hong, W. Jin, H. L. Ho, C. Wang, S. Gao, Y. Wang, and P. Wang, Opt. Express **28**, 5423 (2020).
11. P. Zhao, Y. Zhao, H. Bao, H. L. Ho, W. Jin, S. Fan, S. Gao, Y. Wang, and P. Wang, Nat. Commun. **11**, 1 (2020).
12. Y. Zhao, Y. Liu, L. Zhang, C. Zhang, J. Wen, and T. Wang, Opt. Express **24**, 6186 (2016).
13. Y. Rao, Y. Wang, Z. Ran, and T. Zhu, J. Light. Technol. **21**, 1320 (2003).
14. G. Humbert, A. Malki, S. Février, P. Roy, and D. Pagnoux, Electron. Lett. **39**, 349 (2003).
15. C. Fu, S. Liu, Z. Bai, J. He, C. Liao, Y. Wang, Z. Li, Y. Zhang, K. Yang, and B. Yu, J. Light. Technol. **36**, 1683 (2018).
16. X. Zhou, S. Shi, Z. Zhang, J. Zou, and Y. Liu, Opt. Express **19**, 6253 (2011).
17. X. Kong, K. Ren, L. Ren, J. Liang, and H. Ju, Appl. Opt. **56**, 4702 (2017).
18. Y. Wang, L. Xiao, D. N. Wang, and W. Jin, Opt. Lett. **31**, 3414 (2006).
19. K. Morishita and Y. Miyake, J. Light. Technol. **22**, 625 (2004).
20. Y. Wang, W. Jin, J. Ju, H. Xuan, H. L. Ho, L. Xiao, and D. Wang, Opt. Express **16**, 2784 (2008).
21. J. Tang, G. Yin, S. Liu, X. Zhong, C. Liao, Z. Li, Q. Wang, J. Zhao, K. Yang, and Y. Wang, IEEE Photon. J. **7**, 1 (2015).
22. Z. Wu, Z. Wang, Y. Liu, T. Han, S. Li, and H. Wei, Opt. Express **19**, 17344 (2011).
23. Y. Wang, D. N. Wang, W. Jin, Y. Rao, and G. Peng, Appl. Phys. Lett. **89**, 151105 (2006).

24. L. Jin, W. Jin, J. Ju, and Y. Wang, J. Light. Technol. **29**, 1707 (2011).
25. J. Reid and D. Labrie, Appl. Phys. B **26**, 203 (1981).
26. D. W. Allan, Proc. IEEE **54**, 221 (1966).
27. P. O. Werle, R. Mücke, and F. Slemr, Appl. Phys. B **57**, 131 (1993).